ADVANCES IN ATMOSPHERIC SCIENCES, VOL. 31, SEPTEMBER 2014, 1009–1021

Sensitivity of ENSO Variability to Pacific Freshwater Flux Adjustment in the Community Earth System Model

KANG Xianbiao*[1,2,3], HUANG Ronghui[1,2], WANG Zhanggui[1,2,3], and ZHANG Rong-Hua[4]

[1]*Center for Monsoon System Research, Institute of Atmospheric Physics, Chinese Academy of Sciences, Beijing* 100190

[2]*University of the Chinese Academy of Sciences, Beijing* 100029

[3]*National Marine Environmental Forecasting Center, State Oceanic Administration, Beijing* 100081

[4]*Key Laboratory of Ocean Circulation and Waves, Institute of Oceanology, Chinese Academy of Sciences, Qingdao* 266071

(Received 19 November 2013; revised 21 January 2014; accepted 24 February 2014)

ABSTRACT

The effects of freshwater flux (FWF) on modulating ENSO have been of great interest in recent years. Large FWF bias is evident in Coupled General Circulation Models (CGCMs), especially over the tropical Pacific where large precipitation bias exists due to the so-called "double ITCZ" problem. By applying an empirical correction to FWF over the tropical Pacific, the sensitivity of ENSO variability is investigated using the new version (version 1.0) of the NCAR's Community Earth System Model (CESM1.0), which tends to overestimate the interannual variability of ENSO accompanied by large FWF into the ocean. In response to a small adjustment of FWF, interannual variability in CESM1.0 is reduced significantly, with the amplitude of FWF being reduced due to the applied adjustment part whose sign is always opposite to that of the original FWF field. Furthermore, it is illustrated that the interannual variability of precipitation weakens as a response to the reduced interannual variability of SST. Process analysis indicates that the interannual variability of SST is damped through a reduced FWF–salt–density–mixing–SST feedback, and also through a reduced SST–wind–thermocline feedback. These results highlight the importance of FWF in modulating ENSO, and thus should be adequately taken into account to improve the simulation of FWF in order to reduce the bias of ENSO simulations by CESM.

Key words: ENSO, freshwater flux, CESM

Citation: Kang, X. B., R. H. Huang, Z. G. Wang, and R.-H. Zhang, 2014: Sensitivity of ENSO variability to Pacific freshwater flux adjustment in the Community Earth System Model. *Adv. Atmos. Sci.*, **31**(5), 1009–1021, doi: 10.1007/s00376-014-3232-2.

1. Introduction

As the most significant interannual variability mode centered in the tropical Pacific, ENSO exerts substantial influences on climate variability and predictability worldwide. By using coupled ocean–atmosphere models, operational ENSO forecasting could reach 3–6 months with reasonable credibility (Cane and Zebiak, 1985; Barnett et al., 1993; Latif et al., 1998; Kirtman et al., 2002; Zhang et al., 2005, 2013; Zhu et al., 2013).

However, large uncertainties and systematic errors still exist in simulations and predictions of ENSO. Much effort has been applied to understand ENSO processes, with various forcings and feedbacks identified. For example, it has long been recognized that the surface wind is the dominant forcing (Bjerknes, 1969), while the heat flux serves as a negative feedback in ENSO cycles. In addition, many other feedbacks having modulating effects on ENSO have also been found, such as the feedback induced by tropical instability waves (TIWs) (Zhang and Busalacchi, 2008) and ocean biology (Zhang et al., 2009).

The freshwater flux (FWF), defined as precipitation minus evaporation, is another important forcing to the ocean, and significant progress has been made regarding our physical understanding and modeling of its effect on ENSO. For example, it has been found that FWF has a direct effect on salinity in the upper ocean, which is closely associated with the density of water, mixed layer depth, mixing, and entrainment, all of which have important influences on the SST (e.g., Carton, 1991; Huang and Mehta, 2004; Zheng and Zhang, 2012; Zheng et al., 2014). Reason (1992) found that a zonal overturning cell is generated by the precipitation anomalies associated with ENSO; this cell acts to enhance the vertical mixing of more saline, cooler water into the mixed layer in the forcing region, and at the same time transport the surface fresher water to other places. Yang et al. (1999) found that, through the change of horizontal advection and vertical mixing, the inclusion of FWF increases the SST by about 0.5 K in the tropical Pacific. By using a hybrid coupled model con-

* Corresponding Author: KANG Xianbiao
Email: xianbiankang@163.com

structed from an OGCM and a simplified atmospheric model, Zhang and Busalacchi (2009) and Zhang et al. (2010) demonstrated that the FWF forcing tends to increase the interannual variability of ENSO. Ham et al. (2012) indicated that freshwater runoff decreases the salinity and makes the mixed layer depth shallower, which reduces the vertical mixing and thus increases the SST. Using a fully coupled ocean–atmosphere GCM, Wu et al. (2010) found that the idealized western tropical Pacific FWF acts to trigger an ENSO-type response in the tropics.

These previous studies are helpful for our understanding of the mechanisms by which FWF forcing can induce a response of the ocean and ENSO cycles. However, most results have been obtained from ocean-only (e.g., Yang et al., 1999) or simplified coupled ocean–atmosphere models (e.g., Zhang and Busalacchi, 2009; Zhang et al., 2012), and thus the effects in fully coupled ocean–atmosphere models still need further investigation. As is well known, over the tropical Pacific, most coupled general circulation models (CGCMs) produce a "double ITCZ" pattern with excessive precipitation off the equator near the date line, which is often connected with overly narrow and excessive SST spreading into the western Pacific too far west (Mechoso et al., 1995). As the dominant component of FWF, such precipitation bias can distort the FWF pattern into the ocean considerably, and ultimately affects the reliability of the simulated ENSO.

Very recently, a new version (version 1.0) of the National Center for Atmospheric Research (NCAR) Community Earth System Model (CESM1.0) was released. The model has been available for use in the scientific community, and is expected to have a variety of applications for Earth system modeling and analyses. However, it is already clear that biases remain in this latest version of the model. In particular, the ENSO variability simulated in the current version is too strong [discussed later with respect to the CSEM1.0 simulations of ENSO]. One obvious source of bias is related to the fact that FWF effects are not adequately represented (see the related analyses below).

In this paper, we evaluate the CESM simulation, with a focus on FWF effects on ENSO variability. The exact purpose of the study is to use CESM1.0 to investigate the sensitivity of ENSO variability to FWF forcing in the Pacific. Specifically, a sensitivity simulation using CESM1.0 is performed in which a simplified empirical correction is applied to the FWF field, and then compared with the control simulation without FWF adjustment. We attempt to identify the possible physical mechanism causing such a modulation of ENSO. A similar method has been used in the Community Climate System Model version 3 (CCSM3) for adjusting the heat flux, and it was found that the simulated SST climatology, the seasonal cycle, and interannual variability of ENSO can be improved significantly (Pan et al., 2011). Unlike the role of heat flux, the effect of FWF on the SST is indirectly and predominantly through the adjustment of ocean internal dynamics; as discussed later in the paper, the FWF correction mainly improves the simulation of interannual variability associated with ENSO.

2. Model, data and methodology

2.1. *Model*

CESM 1.0 is a coupled climate model for simulating the Earth's climate system developed from the Community Climate System Model version 4 (CCSM4) (Gent et al., 2011) at the NCAR. The CESM has five separate components simultaneously simulating the Earth's atmosphere, ocean, land, land ice, and sea ice, plus one central coupler. The atmosphere component is version 5 of the Community Atmosphere Model (CAM5) (Gettelman et al., 2010; Neale et al., 2010), with the finite volume dynamical core at a horizontal resolution of 1.9° (lat) $\times$ 2.5° (lon), and 30 vertical layers arranged in a hybrid pressure sigma coordinate. Version 4 of the Community Land Model (CLM4) (Oleson et al., 2010) is used, which shares the same horizontal grid as CAM5. The ocean component is the Parallel Ocean Program version 2 (POP2) (Smith et al., 2010), possessing 60 layers in the vertical direction. The sea ice component is version 4 of the Los Alamos sea ice model (CICE4) (Hunke and Lipscomb, 2008), which is designed specifically to be compatible with POP and has a horizontal resolution of approximately 1°. In addition, the ice sheet component is taken from the Glimmer Community Ice Sheet Model (Glimmer-CISM) (Rutt et al., 2009), with a horizontal resolution of 5 km. CESM1.0 is a useful tool used worldwide by climate researchers in a variety of fields.

2.2. *Observational datasets*

The monthly precipitation (P) data are from the Global Precipitation Climatology Project (GPCP) (Adler et al., 2003), and the monthly evaporation data (covering the period 1979–2008) are from the Objectively Analyzed Air–Sea Fluxes (OAFlux) project (Yu and Weller, 2007). The P and E data are used to derive the FWF fields, defined as P minus E ($P - E$), the value of which is positive when the ocean gains water from the atmosphere, and negative when there is water loss from the ocean surface. Although large uncertainties exist in the precipitation and evaporation data among different observational datasets, especially over the open ocean where no comprehensive *in situ* observations are available for validation (Yang et al., 1999; Schlosser and Houser, 2007; Andersson et al., 2011), the main focus of the current paper is to evaluate how the SST responds to a minor correction of the FWF; the aim is not to examine the sensitivity to the variation in FWF observations, and so we simply adopt the widely used GPCP-OAFLUX datasets as the observations in this study.

The observed SST field is taken from Hurrell et al. (2008) and is used to validate the model results. It comprises the merged products of HADISST1 [Met Office Hadley Centre sea ice and sea surface temperature dataset (1870 onward)] and OI.v2 [National Oceanic and Atmospheric Administration (NOAA) Optimum Interpolation SST version 2 dataset (November 1981 onward)].

2.3. *Corrected FWF scheme*

The equation governing the sea surface salinity ($S_{\rm sur}$) can be written as

$$\frac{\partial S_{\rm sur}}{\partial t} \propto S_{\rm D} + S_{\rm src} \ . \tag{1}$$

As expressed, the tendency of $S_{\rm sur}$ is composed of two parts: the first represents the oceanic process terms ($S_{\rm D}$) that include the horizontal and vertical salt advection, entrainment and sub-scale salt diffusion. The second is associated with the net local FWF at the air–sea, ice–sea and sea–land interfaces, which includes the combined effects of precipitation, evaporation, runoff, sea ice freezing, melting, and so on. In the CESM, the salt flux exchange ($S_{\rm src}$) is processed as converting the FWF to the virtual salinity flux by assuming the ocean reference salinity ($S_0 = 34.5$ psu). This type of experimental setup allows us to focus merely on the salinity effects by purposely leaving the latent heat flux unrestricted to reserve the global surface heat balance. Equation (1) can then be written as

$$\frac{\partial S_{\rm sur}}{\partial t} \propto S_{\rm D} + S_0 \times F \ , \tag{2}$$

in which F is the modeled FWF at the sea surface. The balance between $S_{\rm D}$ and $S_{\rm src}$ determines the patterns of mean $S_{\rm sur}$ in the long-term mean ($\partial S_{\rm sur}/\partial t \sim 0$). The bias of model SSS can be attributed to the errors of $S_{\rm src}$ and $S_{\rm D}$. In this study, we mainly focus on the effects of the systematic error of $S_{\rm src}$ on the ENSO phenomenon, because such error is significant due to the commonly noted deficiency of precipitation simulation in the CESM, especially over the equatorial Pacific, where large FWF error determined by the difference of $P-E$ is still large. To understand the effect of such error sources, a time-dependent FWF adjustment term is added to F in Eq. (2) to compensate for the systematic error:

$$\frac{\partial S_{\rm sur}}{\partial t} \propto S_{\rm D} + S_0 F_{\rm flx} \ ; \tag{3}$$

$$F_{\rm flx} = F_{\rm mod} + F_{\rm adj} \ ; \tag{4}$$

$$F_{\rm adj} = \alpha (F_{\rm obs} - F_{\rm mod}) \ . \tag{5}$$

Here, $F_{\rm mod}$ is the original FWF, calculated as $P-E$ at the sea surface; $F_{\rm obs}$ is the observed FWF, obtained by linearly interpolating the observed (GPCP-OAFLUX) long-term monthly mean (1979–2008) FWF to each time step (1-day interval) of air–sea coupling; and $F_{\rm adj}$ is an adjustment term, defined by multiplying a coefficient (α) to the difference between $F_{\rm obs}$ and $F_{\rm mod}$. In the current study, the FWF adjustment is only applied to the tropical Pacific Ocean (30°S–30°N, 120°E–70°E) where the observational FWF datasets are available and the effects of FWF bias on ENSO are of great interest, with the adjustable coefficient arbitrarily denoted as 1/30 and kept constant over the region. By doing so, the systematic bias of FWF can be effectively reduced.

In this paper, we first conduct the FWF-unadjusted IPCC/CMIP5 (Intergovernmental Panel on Climate Change/Coupled Model Intercomparison Project Phase 5) long-term historical run, during which the CESM is forced by atmospheric composition variations including both natural and anthropogenic sources, with land cover set to be time-evolving (Taylor et al., 2011). The historical run is initiated from the preindustrial quasi-equilibrium control run, and is integrated from 1850–2005; such an experiment is also termed a "20th century" simulation because it integrates from the mid-19th century to near the present day (covering much of the industrial period). This experiment is the control run and referred to as CTL hereafter. A sensitivity experiment (referred to as FLX hereafter) is then conducted using the above FWF adjustment scheme. The FLX simulation is initiated from the state determined from the CTL simulation on 1 January 1901 and integrated for 105 years. The first 45 years are used to spin up and the results of the remaining 60 years (1946–2005) are used to conduct the following analyses. Note that different values of α have been tested and it is found that, although different values of α indeed have an influence on the signal strength, it is unlikely that this affects the quality of the current conclusion. In addition, the constant α over the whole region does not cause an abrupt change in salinity near the transitional area, and therefore also does not impede the following results.

3. The standard CESM1.0 simulation

The interannual variability of freshwater flux anomaly (FWFA) in the equatorial Pacific is closely correlated with ENSO cycles. During El Niño years, large positive FWFA dominates the western and central equatorial Pacific, which is attributed to the intense precipitation associated with the eastward movement of maximum sea surface temperature anomaly (SSTA). The situation for the La Niña years operates in an opposite way, in which negative FWFA appears in the western and central equatorial Pacific. Figure 1 compares the observational interannual variability of FWFA along the equator with that in the CTL experiment. Compared to the observation (Fig. 1a), the FWFA variability along the equatorial Pacific tends to be overestimated significantly in the CTL experiment (Fig. 1b). Specifically, during El Niño years, the FWFA in the CTL experiment has larger values and extends more eastward than that in the observation. This can further be demonstrated in Fig. 2 where the FWFA standard deviation in the CTL experiment (Fig. 2b) is generally about 0.5 mm $\rm d^{-1}$ larger than that in the observation (Fig. 2a), especially over the western Pacific warm pool and along the ITCZ and South Pacific convergence zone (SPCZ).

Figure 3 shows the long-term annual mean FWF over the tropical Pacific from the models and observation. In observations (Fig. 3a), most of the positive FWF occurs in the western Pacific warm pool, northern ITCZ along 5°N, and SPCZ, where the SST is warm, the convection is active, and the associated intense precipitation is the main contributor to FWF. Correspondingly, much negative FWF is located besides the north of the ITCZ, eastern edge of the warm pool, and SPCZ. In these areas, the SST is usually lower than 27°C, meaning less convection can be triggered, the precipitation is low, and evaporation is the dominant contributor to FWF. The CTL experiment successfully captures the position of positive FWF in the warm pool, along the ITCZ and SPCZ, and

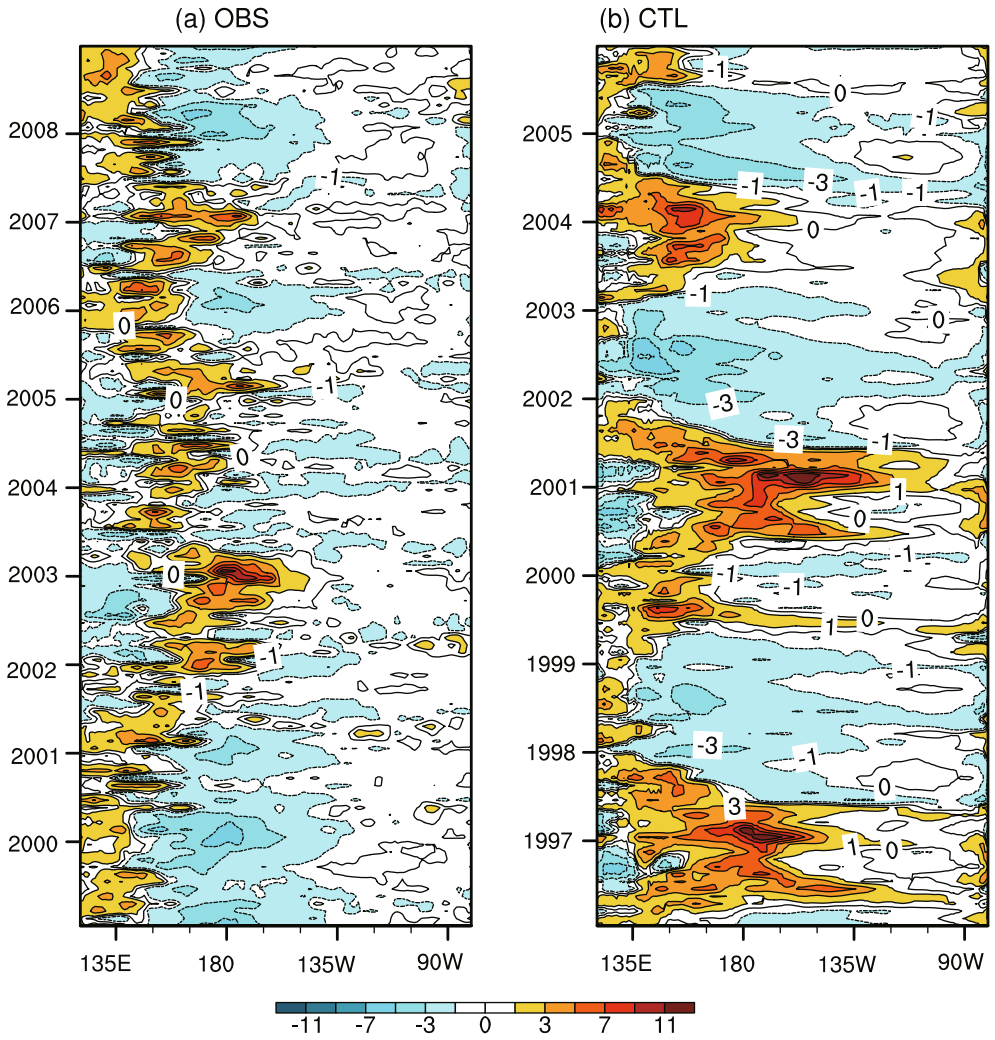

Fig. 1. Time–longitude sections of FWFA(F') in the equatorial (5°S–5°N) Pacific for the (a) observation; (b) CTL experiment. The contour interval is 2 mm d^{-1} for $F' \geqslant 1.0$ (or $F' \leqslant -1.0$) mm d^{-1}.

the negative FWF center north of the ITCZ (Fig. 3b). However, the simulated FWF is too weak in the warm pool, too strong in the ITCZ, and too strong and extended too far east in the SPCZ (Fig. 3e). The eastern extension of the stronger SPCZ tends to split the whole negative FWF center in the central-southeastern Pacific (Fig. 3a) into two parts: one center in the equatorial central eastern Pacific, and another in the southeastern Pacific (Fig. 3b). This deficiency of FWF simulation can be mainly attributed to the "double ITCZ" problem, which is a commonly noted bias in CGCMs, and remains a challenge for the state-of-the-art CESM1.0.

Figure 4 shows the spatial distributions of the standard deviation of interannual SST anomalies for the observations and the CTL experiment. The maximum values (1.25°C–1.5°C) of the observed SST variations are found near the equatorial eastern Pacific, with decreasing amplitude extending westward to 130°W (Fig. 4a). In comparison to this, the simulated maximum values in the CTL experiment reach 1.75°C–2.0°C, with an unrealistic center around 120°W. Another apparent discrepancy in the control run is the equatorial interannual SST anomalies extending too far west, and the slightly overestimated SST anomalies in the subtropics (Fig. 4b). To further quantify the variability of SST simulations, we summarize the standard deviation of each Niño index in Table 1. The interannual variability of SST tends to be overestimated significantly along the equatorial Pacific. For example, the standard deviation of SST variability in CTL (OBS) is 1.22 (0.66) in the Niño4 area, 1.49 (0.85) in the Niño3.4 area, and 1.45 (0.88) in the Niño3 area. In contrast, the SST variability in the Niño1+2 areas is slightly underestimated in the CTL experiment, with its standard deviation being 1.0 in the CTL experiment, and 1.07 in the observation.

To illustrate the time evolution of SSTA related to ENSO, the Niño3 index for the CTL experiment is shown in Fig. 5b, in comparison with the index derived from the observed SSTs (Fig. 5a). Note that the El Niño years in the experiments can only by coincidence match observations because of their differences of the initial internal variations between the experiments and observation. The initial conditions of the historical runs are taken from an arbitrary point of a quasi-equilibrium

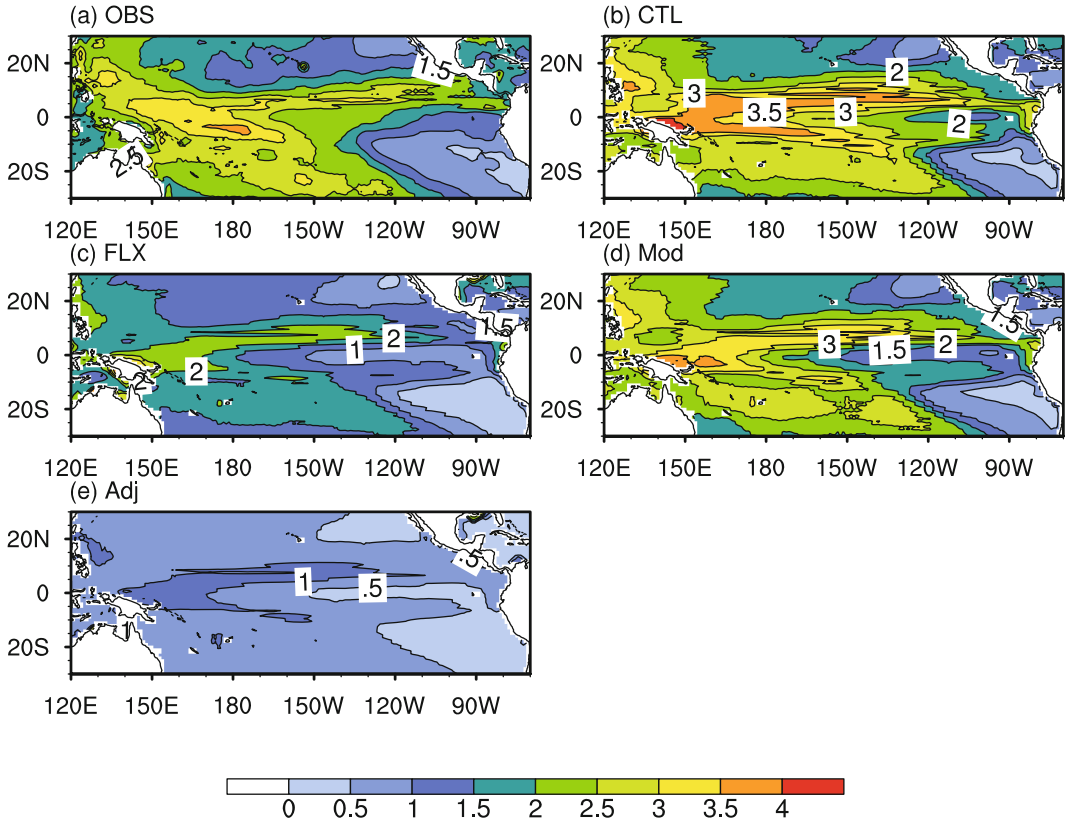

Fig. 2. Spatial distributions of the standard deviation for FWFA over the tropical Pacific: (a) observation; (b) CTL; (c) F_{flx}; (d) F_{mod}; (e) F_{adj}. The contour interval is 0.5 mm d^{-1}.

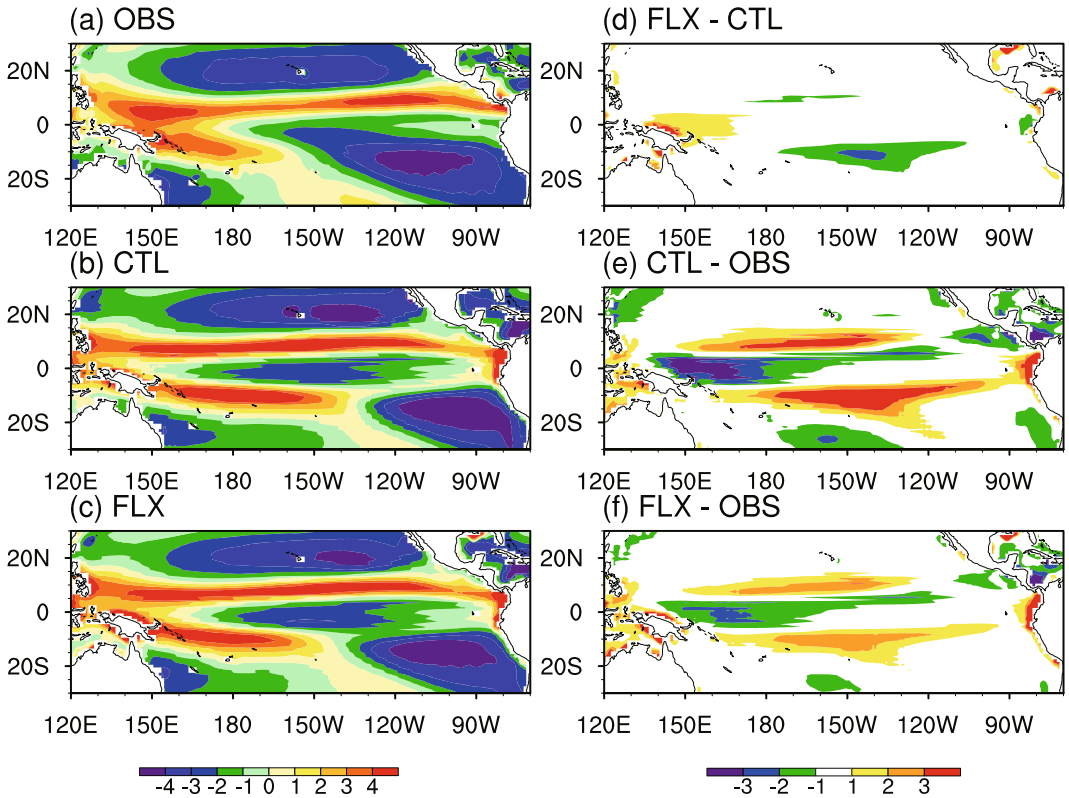

Fig. 3. Spatial distributions of the long-term annual mean for FWF (F): (a) observation; (b) CTL; (c) FLX; (d) difference between FLX and CTL; (e) bias in CTL; (f) bias in FLX. The contour interval in (a–c) is 1.0 mm d^{-1}, and in (d–f) is 1.0 mm d^{-1} for $F \geqslant 1.0$ ($F \leqslant -1.0$) mm d^{-1}.

Table 1. Standard deviations of the observed Niño indices, and those of the CTL and FLX experiments. The numbers in brackets along the CTL row denote the overestimated percentage of the Niño indices in the CTL experiment relative to that observed. The first of the two numbers in brackets along the FLX row denotes the overestimated percentage of the indices in FLX experiment relative to that observed, while the second of the two denotes the decreased percentage of the indices in the FLX experiment relative to that in CTL experiment.

	Niño4	Niño3.4	Niño3	Niño1+2
OBS	0.66	0.85	0.88	1.07
CTL	1.22 (85%)	1.49 (75%)	1.45 (65%)	1.0 (−6%)
FLX	1.01 (53%, −17%)	1.1 (29%, −26%)	1.02 (16%, −30%)	0.71 (−33%, −29%)

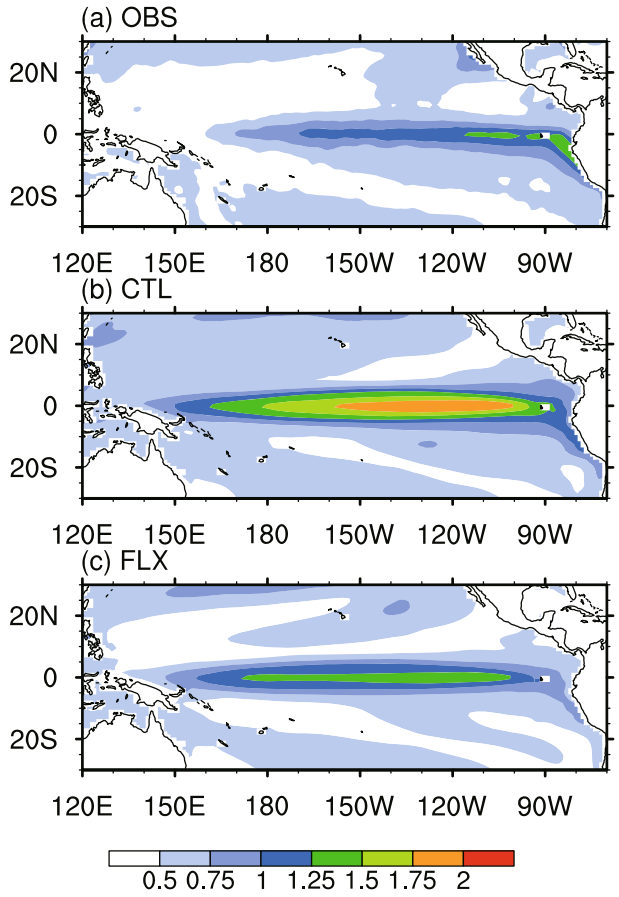

Fig. 4. Spatial distributions of the standard deviation for SST anomalies over the tropical Pacific: (a) observation; (b) CTL; (c) FLX. The contour interval is 0.25°C.

control run (Taylor et al., 2011). The different characteristics of ENSO in the experiments and observations can be seen clearly by visual inspection of the time series. The Niño3 index in the CTL experiment (Fig. 5b) is characterized by a quasi-regular 2-yr cycle, while that of the observation is more irregular (Fig. 5a). Additionally, during the mature phase of El Niño (La Niña) events, most of the SSTA in the CTL experiment is greater (less) than 2.0°C (−2.0°C) (Fig. 5b). In contrast to this, it is usually less (greater) than 2.0°C (−2.0°C) in the observation (Fig. 5a), indicating that the interannual variability of SST has been significantly overestimated in the CESM control run.

Figure 6 presents the power spectrum (based on the continuous Fourier method) of the 60-yr Niño3 index for the observation and experiments. The observation shows periods from 1.2 years to 4.5 years, which is significantly larger than the red noise process at the 95% confidence level (based on the chi-squared table). The dominant 4-year period shown in the observations is reproduced well in the control run; however, the spectral intensity has been overestimated significantly, with about 24% (12%) in the CTL experiment (observation). There is a distinct and robust quasi-biennial oscillation (also shown in Fig. 5b) in the CTL experiment, which is a long-standing deficiency of CCSM3 and CCSM4 (Deser et al., 2006), but still exists in the current version of the CESM.

In summary, when using the standard CESM1.0, the simulated long-term annual mean FWF has an obvious "double-ITCZ" type bias. The simulated interannual variability of SST and FWF in the equatorial Pacific is too strong, clearly indicating that the ENSO variability tends to be overestimated in CESM1.0 (by more than 65%, as indicated in the Niño3 index; Table 1).

4. The effect of the FWF correction

To reveal what benefit can be gained by the FWF correction, a perturbation run (i.e., FLX) is conducted. In this study, the correction is applied only to the tropical Pacific (30°S–30°N, 120°E–80°W). As the only difference between the CTL and FLX experiment is the specification of the FWF, the effects of FWF on ENSO can be isolated in a clean way. Specific questions to be addressed are: How does the CESM1.0 respond to the FWF correction? Is there any significant effect on ENSO? Is the effect positive or negative in terms of ENSO amplitude? What benefit can be gained by climate modeling using the CESM1.0 with the improved FWF? Can the CESM1.0 biases be reduced by including the FWF correction? Can ENSO variability be reduced? Are the processes involved in the CESM1.0 the same as those identified in previous simplified (hybrid) coupled modeling experiments (e.g., Zhang and Busalacchi, 2009; Zhang et al., 2010, 2012)?

Figure 7 shows the FWFA (F') and its correction terms along the equator [as written in Eq. (4)] in the FLX experiment. The sign of adjustment of the freshwater flux anomaly part (F'_{adj}) is always opposite to that of the original freshwater flux anomaly part (F'_{mod}), indicating that the correction always acts to reduce the interannual variability of F'_{mod} during ENSO cycles. During strong El Niño (e.g., the period 1998–99 in Fig. 7a) or La Niña (e.g., the period 2000–01 in Fig. 7a)

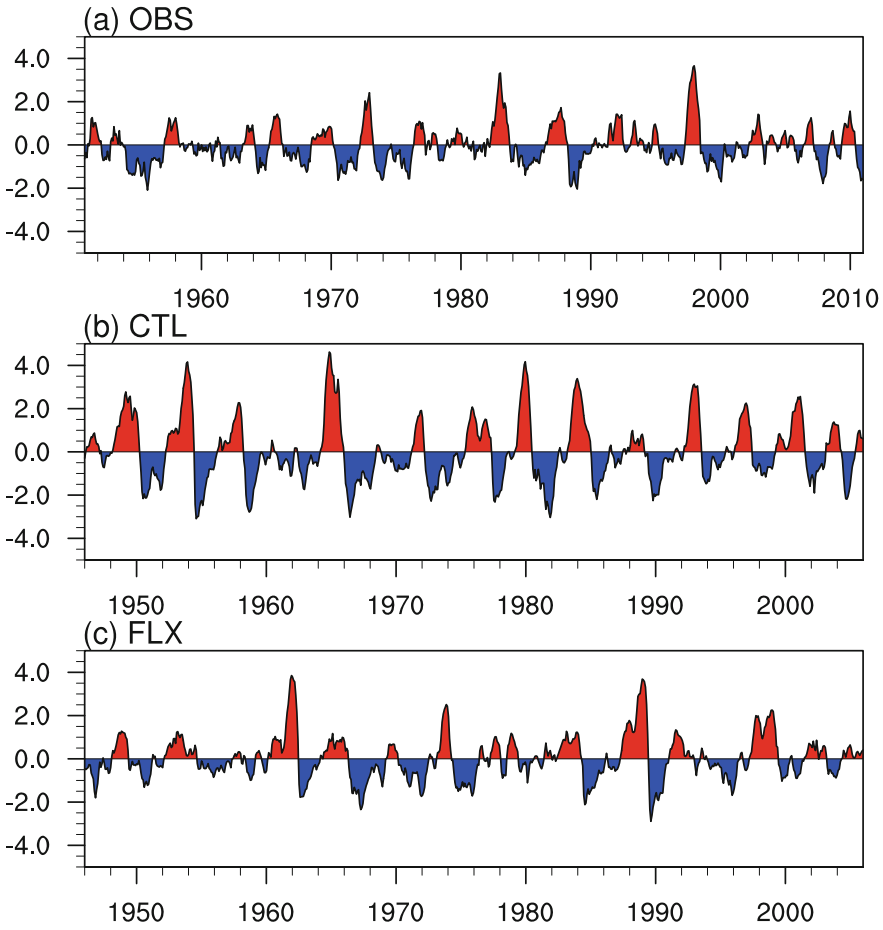

Fig. 5. Time series of the Niño3 index for (a) observation; (b) CTL; (c) FLX.

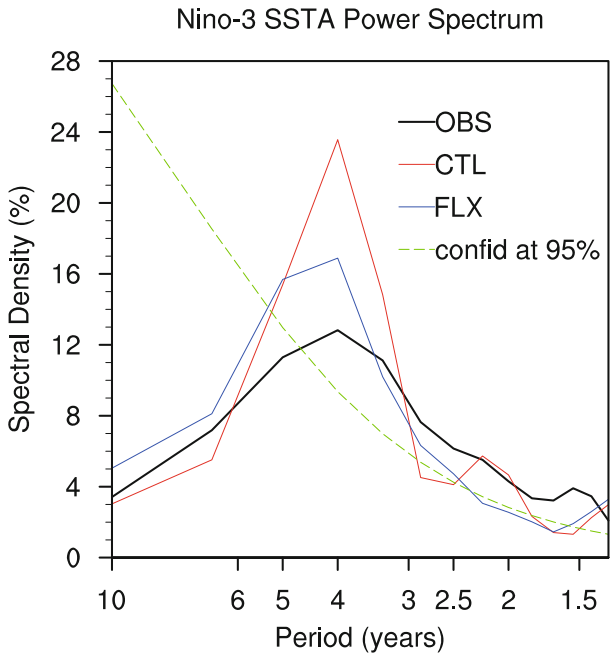

Fig. 6. Power spectrum period of the Niño3 index calculated from 60-yr SST data for observation (black), CTL (red), and FLX (blue). The green dashed line indicates the upper limit of the 95% confidence level.

phenomena, the amplitude of F'_{adj} is also bigger, acting to have more of a correcting effect on F'_{mod}; while in normal years, the F'_{adj} amplitude is much lower and has less effect on F'_{mod}. The compensating effects of these two items lead to a significant reduction of the actual freshwater flux anomaly (F'_{flx}) into the ocean in the FLX experiment (Fig. 7c), as compared to that in the CTL experiment (Fig. 1b). Such effects are not just confined within the equatorial Pacific, but occur over the whole tropical Pacific where the adjustment method is being applied. This can also be demonstrated in the spatial distribution of the standard deviation of FWFA (Fig. 2). The standard deviation of FWFA is 2.5–3.5 mm d^{-1} over the SPCZ, and more than 3.5 mm d^{-1} over the ITCZ and western Pacific warm pool in the CTL experiment (Fig. 2b). In contrast to this, it is much lower during the FLX experiment: 1.5–2.0 mm d^{-1} over the SPCZ, and 1.5–2.0 mm d^{-1} over the ITCZ and western Pacific warm pool (Fig. 2c).

The effects of FWF adjustment on the long-term annual mean FWF are shown in Fig. 3c. Although the position of the simulated FWF has not obviously improved in the FLX experiment (Fig. 3c), the amplitude of the bias has indeed been effectively reduced (Figs. 3d and f). For example, the large positive FWF bias center east of the SPCZ has been reduced by 1–2 mm d^{-1}; the large negative bias center in the equatorial western Pacific (0°N, 155°E) has also been decreased by

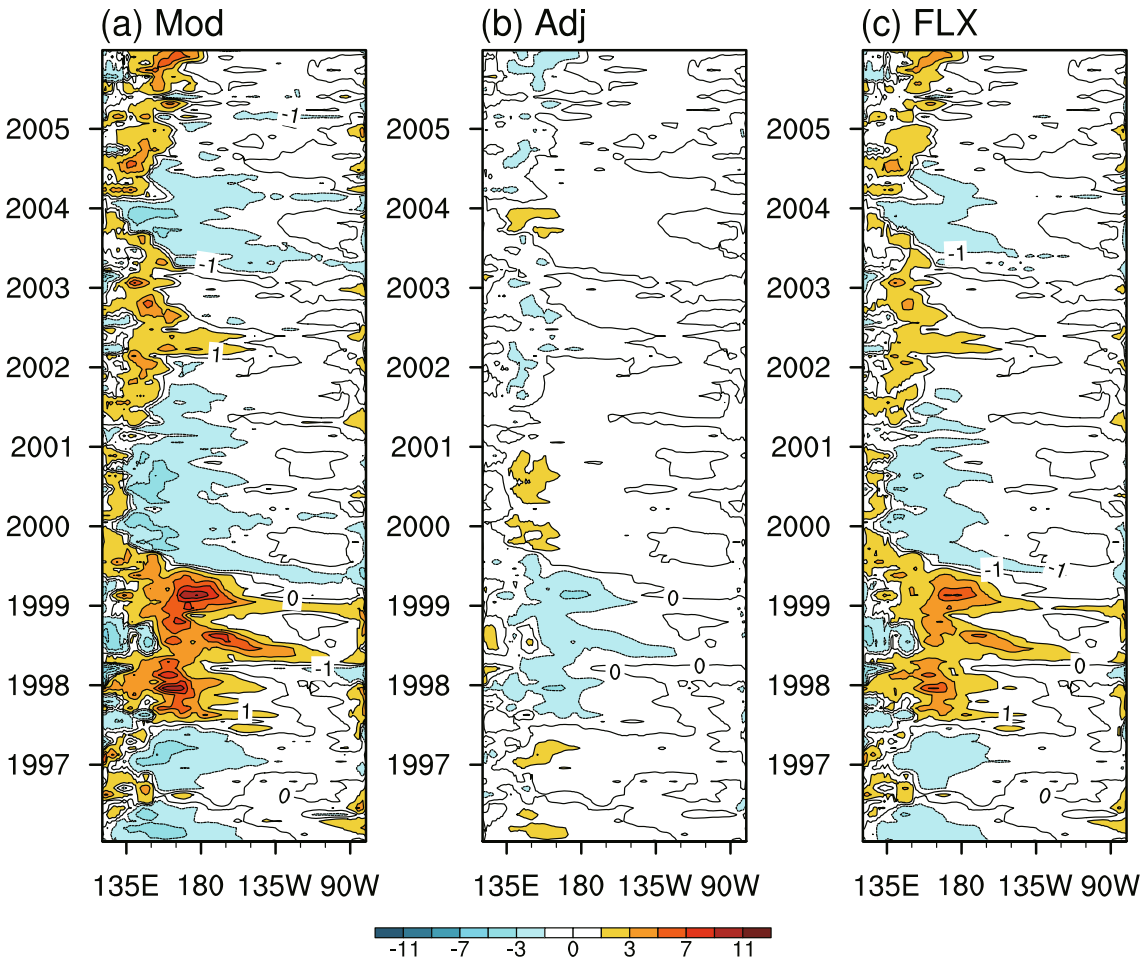

Fig. 7. Time–longitude sections of the FWFA (F') terms [as written in Eq. (4)] over the equatorial Pacific (5°S–5°N) for the FLX experiment: (a) the original FWFA ($F'_{\rm mod}$); (b) the adjusted FWFA ($F'_{\rm adj}$); (c) total FWFA into the ocean ($F'_{\rm flx}$). The contour interval is 2.0 mm d^{-1} for $F' \geqslant 1.0$ (or $F' \leqslant -1.0$) mm d^{-1}.

1–2 mm d^{-1} (Figs. 3d and f). Some other improvements can be seen over the ITCZ area, with FWF into the ocean being slightly reduced by about 1 mm d^{-1} (Fig. 3d).

Compared with that in the CTL experiment, the patterns of simulated long-term annual mean SSTs have not changed considerably in the FLX experiment. The warm bias along the Peru coast and too strong cold tongue over the central and eastern equatorial Pacific are still large (figures omitted). This is reasonable considering that the effect of FWF on SST is not as significant as that of wind stress associated with the dominant wind–SST–thermocline feedback mechanism in the tropical Pacific.

The patterns of standard deviation for simulated SSTs in the FLX experiment are very similar to those in the CTL experiment. However, the value in the FLX experiment is much lower and closer to the observation (Fig. 4c and Table 1), especially in the equatorial Pacific, where the standard deviation in the FLX experiment has only been overestimated by 16% of Niño3, 29% of Niño3.4, and 53% of Niño4; in comparison to 65% of Niño3, 75% of Niño3.4, and 85% of Niño4 in the CTL experiment (Table 1). It can also be seen that the maximum percentage adjustment mainly occurs over the eastern Pacific (−29% in the Niño1+2 area and −30% in the Niño3 area); while in the central and western Pacific, the corrected percentage is relatively lower (−26% in the Niño3.4 area and −17% in the Niño4 area) (Table 1). Furthermore, in the western and central subtropics, the standard deviation is less than 0.5°C in the FLX experiment, which is closer to the observation than that in the CTL experiment (Fig. 4c).

As shown in Fig. 6, the blue line locates besides the left of the red line, indicating that the low frequency at the interannual variability scales tends to be enhanced, while the high frequency is likely to be suppressed in the FLX experiment. The overall range under the blue line is much less than that under the red line and is closer to that under the black line, suggesting that the amplitude of the interannual variability has been effectively reduced by applying FWF correction methods, consistent with the result obtained from the standard deviation distribution in Fig 4. Also, the peak of the spectral density at four years has been reduced effectively by 30% in the FLX experiment. Furthermore, it is surprising to note that the variations of Niño3 index are more irregular, and the quasi-biennial oscillation bias existing in the control run has been effectively diminished in the FLX experiment.

All these results clearly indicate that various aspects of the simulation of ENSO can be affected significantly by applying an FWF correction in the FLX experiment, although the climatological fields of FWF and SST seem to be influenced only a little. In particular, the interannual variability of SST and FWF are significantly reduced when the FWF correction is applied, with the standard deviation of Niño3 index (Table 1) being reduced from 1.45°C in the CTL experiment to 1.02°C in the FLX experiment (>30%), indicating that the FWF effects need to be adequately represented in the CESM1.0 because they act to significantly reduce the ENSO variability.

5. Process analyses of the effects induced by the FWF correction

By using a simplified ocean–air coupled model, Zhang and Busalacchi (2009) discussed in detail the physical processes associated with FWF. They found that the FWF can exert a direct influence on two parameters (SSS and buoyancy flux) in the ocean. The SSS is closely connected with the oceanic density field, which is an important factor influencing the vertical mixing and stability of the upper ocean. The buoyancy flux, which is a combination of the net heat flux and freshwater flux at the sea surface, acts as a forcing to the ocean, and controls the evolution of mixed layer depths (MLDs). Together with the wind stress and heat flux, FWF can affect the entrainment of the mixed layer, thus influencing the SST. However, in the current study, the FWF is converted to the virtual salt flux, which serves as the source/sink of salt for the salt conservation equation, and the processes of FWF correction on the SST are discussed in detail in the following. In order to more clearly depict the coherent relationships between interannual anomalies of various oceanic and atmospheric fields during ENSO cycles, a composite analysis is conducted in the following. The composite warm (cold) ENSO event is constructed by averaging all the warm (cold) years. The warm (cold) years are defined according to the criterion that the averaged Niño3 index for five consecutive months from October to February (in the following ENSO year) is greater (less) than or equal to 0.75 (−0.75) its standard deviation over the 60-yr period. Following this process, there are 15 (17) warm (cold) events in the observations, 14 (17) in the CTL experiment, and 15 (15) in the FLX experiment. Other alternative composite methods are also tested, such as choosing a different criterion of standard deviation or averaging over different months centered on December, and it is found that the following results are not affected.

The spatial patterns of various anomaly fields in the CTL run are shown in Fig. 8. During El Niño, warm SSTA appears in the central and eastern basin (Fig. 8a), accompanied with large positive FWFA in the equatorial Pacific, SPCZ, and ITCZ (Fig. 8b). The direct effect of the positive FWFA is to reduce SSS (Fig. 8c) in the central and western Pacific. Correspondingly, the surface ocean density becomes less (Fig. 8d), which tends to stabilize the upper ocean and depress the mixing at the base of the mixed layer. Accompanied with this, the MLD becomes shallower in the western and central equatorial Pacific, which also tends to suppress the entrainment of subsurface water into the mixed layer (Fig. 8e). These oceanic processes are favorable for the warming in the surface layer, which have also been demonstrated in Zhang and Busalacchi (2009).

The anomaly fields in the FLX experiment (Fig. 9) are compared to those in the CTL experiment (Fig. 8). There is less positive FWFA into the ocean in the western and central equatorial Pacific (Fig. 9b), leading to the relatively lower SSS anomaly (Fig. 9c) in comparison to the situation in the CTL experiment (Fig. 8c). The lower freshwater amount acts to cause greater surface ocean density in the FLX experiment (Fig. 9d), which makes the upper ocean less stable and thus conducive to stronger mixing of cold water into the mixed layer, leading to stronger cooling of SST during El Niño events in the FLX experiment (Fig. 9a). As a result, less positive SST anomalies can be seen in the FLX experiment (Fig. 8a).

Further, the air–sea system is a coupled system; the effect of FWF on SST is reinforced through a damped Bjerknes feedback (Bjerknes, 1969). The less warming of SST due to the enhanced vertical mixing in the FLX experiment tends to reduce the zonal wind stress anomalies (figures not shown). This acts to make the MLD less shallower in the central and western equatorial Pacific (Fig. 9e compared with Fig. 8e), which is favorable for more entrainment of cold water below the mixed layer into the upper ocean, and thus suppresses the warming in the FLX experiment compared to that in the CTL experiment (Fig. 9a).

The FWF adjustment term acts to dampen the interannual variability in the FLX experiment via two routes. First, the $F'_{\rm adj}$ directly reduces the variability of $F'_{\rm flx}$, since its sign is always opposite to that of $F'_{\rm mod}$ (Fig. 7). Second, the weakened SST anomalies caused by the FWF correction through the mechanism discussed above, act to reduce the precipitation into the ocean. Since precipitation is the main contributor to the FWF in the western and central Pacific, the reduced precipitation leads to a decrease in $F'_{\rm mod}$ (Fig. 7a) and thus a further reduction in $F'_{\rm flx}$. Therefore, the small FWF correction, as seen for the amplitude of $F'_{\rm adj}$ (Fig. 7b), results in a significant effect on interannual variability in the FLX run. For example, as shown in Fig. 7b, the $F'_{\rm adj}$ is about 1 mm d^{-1} in the western and central Pacific during El Niño, which is nearly one order of magnitude smaller than the FWF itself (about 9 mm d^{-1}) in the CTL experiment (Fig. 1b). However, as seen above, even such a small $F'_{\rm adj}$ term can lead to the amplitude of $F'_{\rm mod}$ in the FLX experiment being about 2 mm d^{-1} lower (Fig. 7a) than the F' in the CTL experiment (Fig. 1b). The decreased $F'_{\rm mod}$ (Fig. 7a), together with the compensating effects of $F'_{\rm adj}$ on $F'_{\rm mod}$ (Fig. 7b), leads to the total $F'_{\rm flx}$ field being significantly damped (Fig. 7c), with the maximum value at about 5 mm d^{-1} compared to 9 mm d^{-1} in the CTL experiment (Fig. 1b). This can also be seen in the spatial distribution of the FWFA standard deviation. The

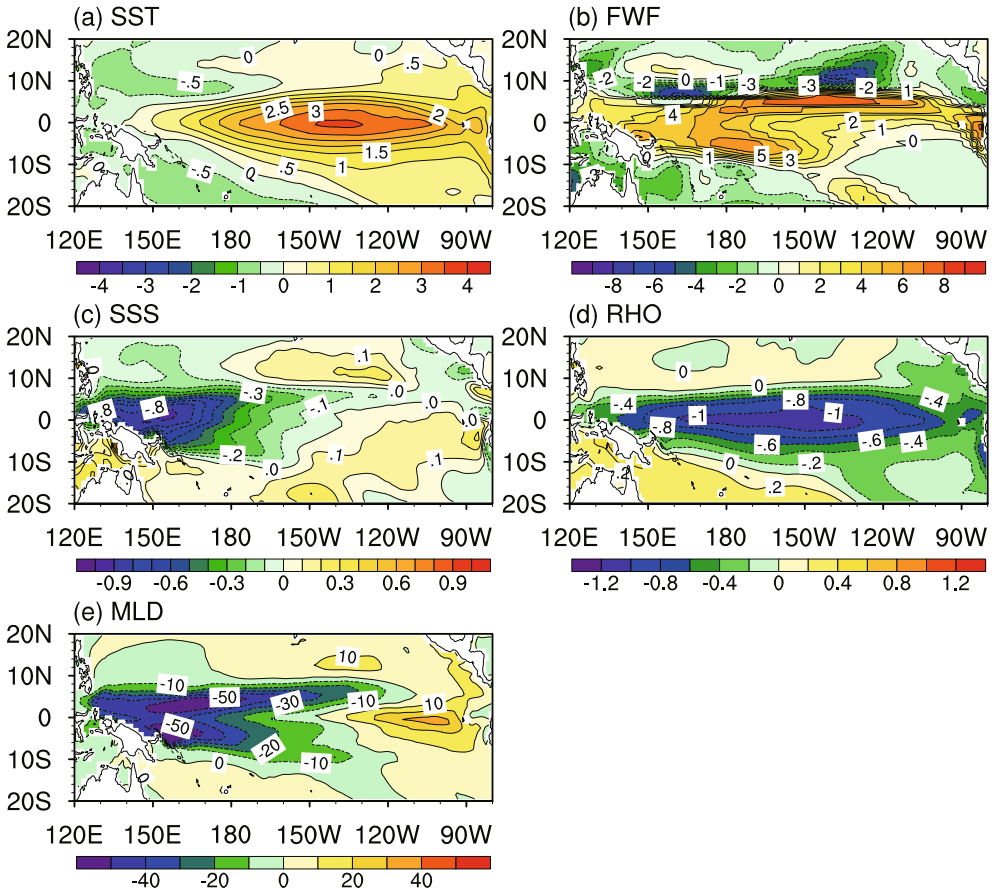

Fig. 8. Spatial distributions for anomalies of composite El Niño events for the CTL experiment in December: (a) SST; (b) FWF; (c) SSS; (d) ocean surface density; (e) MLD. The contour interval is (a) 0.5°C, (b) 1.0 mm d^{-1}, (c) 0.1 psu, (d) 0.2 kg m^{-3}, and (e) 10.0 m.

standard deviation of F_{adj} anomalies is approximately 1 mm d^{-1} in the ITCZ, SPCZ, and western equatorial Pacific regions (Fig. 2e), which is smaller than that of FWFA (>3.5 mm d^{-1}) in the CTL experiment (Fig. 2b). However, such FWF adjustment can decrease the standard deviation of F_{flx} anomalies maximally to 2.0 mm d^{-1}, which is partly through its own compensating effects (Fig. 2d), and partly through reducing the standard deviation of F_{mod} anomalies to about 1.0 mm d^{-1} (Fig. 2e).

The situation for La Niña operates via a similar mechanism, but in an opposite way. That is, the cooling of SST during La Niña tends to be suppressed due to the FWF adjustment (figures omitted).

Therefore, the FWF adjustment acts to weaken the interannual variability of SST through reducing that of FWF during ENSO cycles. As the sign of F'_{adj} is always opposite to that of F'_{mod}, F'_{flx} is directly reduced during ENSO evolution. The reduced variability of FWF acts to have direct effects on SSS, which further influence the density, and then the stability of the mixed layer, the mixing, and entrainment; the modulated ocean processes act to reduce the variability of SST. The damped effects on SST can be further strengthened through SST–wind–thermocline positive feedback. The air–sea interaction is fully coupled in the current study and the reduced variability of SST tends to reduce that of precipitation. This then further reduces the interannual variability of F'_{mod}, and thus exaggerates the damping effects of FWF adjustment on the interannual variability of total FWF into the ocean.

6. Concluding remarks

Realistic ENSO simulations are still a challenging issue in CGCMs; various model factors have been identified that can affect ENSO variability in the tropical Pacific climate system, such as wind, heat flux, ocean biology, and TIWs. In recent years, the role played by FWF in ENSO has been of increased interest due to its significant effects on the ENSO phenomenon. Current CGCMs have common systematic bias in FWF; however, the extent to which the FWF bias can influence ENSO simulations in CGCMs has not been evaluated in a clear way. In this study, the latest CESM (version 1.0) is used to examine the effect induced by the bias of FWF into the tropical Pacific. In particular, we identify the influence of FWF exerted on the simulation of ENSO, and analyze the possible physical mechanism involved. The main results can be summarized as follows: (1) By applying the FWF adjustment method, the bias in interannual variability of FWF is

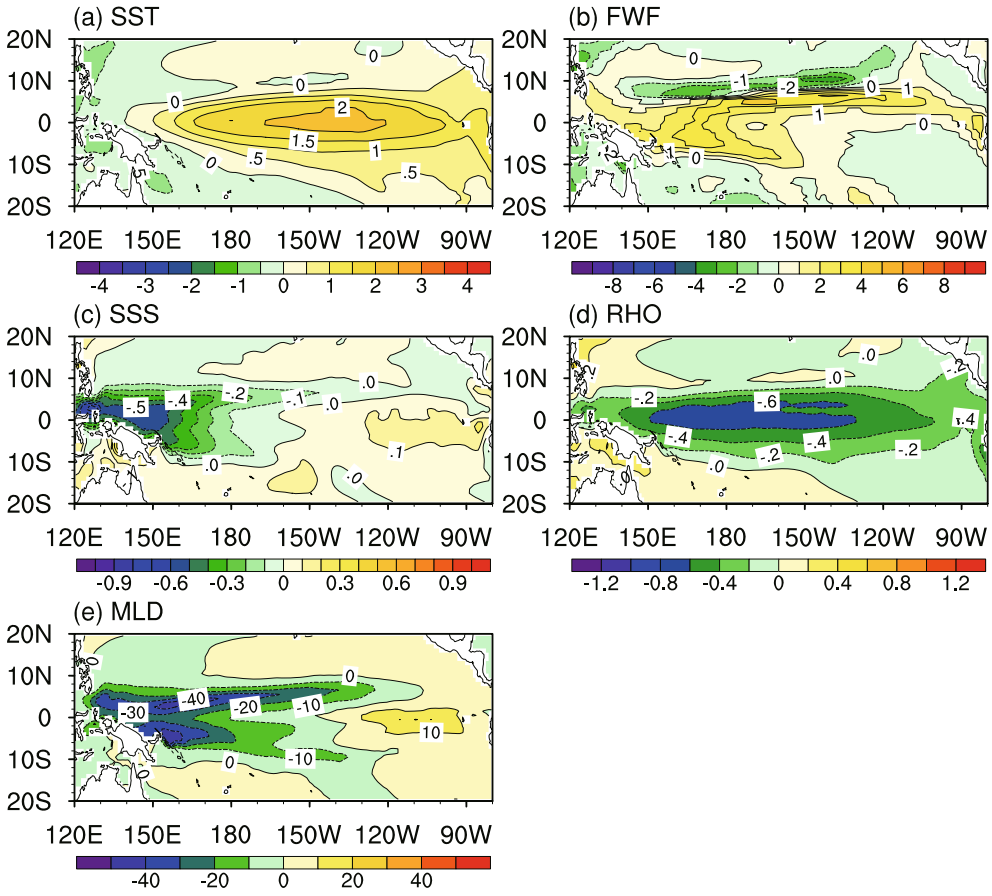

Fig. 9. Spatial distributions for anomalies of composite El Niño events for the FLX experiment in December: (a) SST; (b) total FWF into the ocean (including the original and adjusted part); (c) SSS; (d) ocean surface density; (e) MLD. The contour interval is (a) 0.5°C, (b) 1.0 mm d^{-1}, (c) 0.1 psu, (d) 0.2 kg m^{-3}, and (e) 10.0 m.

effectively reduced during ENSO cycles; (2) Accompanied with this, the too strong bias of interannual SST variability is also significantly reduced; (3) The reductions for biases of FWF and SST in climatological fields are less obvious because the long-term mean fields of FWF correction are almost zero.

The mechanism involved with the FWF effects on ENSO can be summarized as follows: during El Niño events, the positive FWFA into the ocean is directly reduced over the western and central equatorial Pacific when adding a restoring term whose sign is always opposite to that of the FWF itself. The reduced positive FWF anomaly during El Niño, which results in less freshening in the upper ocean, acts to make the mixed layer less stable and enhance the mixing and entrainment of cold water into the mixed layer. These induced oceanic processes act to suppress the warming of SST during El Niño. Such effects can be further amplified through the SST–wind–thermocline feedback, in which the weakened SST anomalies, themselves due to the enhanced vertical mixing induced by the less FWF into the ocean, lead to a reduced zonal wind stress, shallower MLD, and thus less warming. Also, the diminished SST warming during El Niño tends to reduce the precipitation, and thus reduce the original FWF (F_{mod}) into the ocean. The situation for La Niña operates with the same processes but in an opposite sense, acting to suppress the cooling of SST. Thus, the interannual variability of SST can be significantly reduced due to a relatively small correction of the FWF.

It is also interesting to note that the FLX experiment additionally leads to a reduction in the 2-yr-period bias on SST, a long-standing problem puzzling the developers of CESM1.0, and also its predecessor in the CCSM series. The reason for this is not the main focus of the current study, but will be discussed in detail in a future paper. Taken together, these improvements clearly highlight the important role played by FWF in the interannual variability in the tropical Pacific. Our results demonstrate that the feedback induced by FWF can make a significant contribution to the interannual variability of ENSO. The results from this CESM1.0-based modeling study are meaningful not only for interpreting the physical mechanisms through which FWF exerts influence on the ENSO phenomenon, but also as an alternative way to improve ENSO simulation in air–sea coupled models. Note that the correction method for reducing the FWF used in the FLX experiment is merely a sensitivity experiment aimed at illustrating the effects that FWF has on ENSO in coupled sys-

tems; we acknowledge that this is not an ideal solution to solve the problem associated with FWF bias and ENSO simulation. Indeed, some characteristics of ENSO become worse in the FLX experiment [e.g., the large variability center in the Pacific is far too west (Fig. 4), and the Niño1+2 variability becomes weak (Table 1)], which together highlight the complex nature of factors influencing ENSO simulation, and the FWF correction cannot be treated as the panacea to solve all problems related to the simulation of ENSO. The best solution for removing the systematic error in FWF is to improve the physical parameterizations governing the air–sea interactions in the coupled models, but this kind of model improvement is a long-term process undertaken by large modeling groups. Nevertheless, the current work is meaningful for providing clear evidence of the sensitivity of ENSO variability to Pacific FWF adjustment, as well as an illustration of the possible underlying physical mechanism.

Acknowledgements. This research was supported by the National Natural Science Foundation of China (Grant Nos. 41230527 and 41375065), and the National Basic Research Program of China (Grant No. 2010CB950403). The authors wish to thank the anonymous reviewers for their numerous comments that helped improve the original manuscript.

REFERENCES

Adler, R. F., and Coauthors, 2003: The version-2 Global Precipitation Climatology Project (GPCP) monthly precipitation analysis (1979–Present). *Journal of Hydrometeorology*, **4**, 1147–1167.

Andersson, A., C. Klepp, K. Fennig, S. Bakan, H. Grassl, and J. Schulz, 2011: Evaluation of HOAPS-3 Ocean Surface Freshwater Flux Components. *J. Appl. Meteor. Climatol.*, **50**, 379–398, doi: 10. 1175/2010JAMC2341.1.

Barnett, T. P., N. Graham, S. Pazan, W. White, M. Latif, and M. Flügel, 1993: ENSO and ENSO-related predictability. Part I: Prediction of equatorial Pacific sea surface temperature with a hybrid coupled ocean-atmosphere model. *J. Climate*, **6**, 1545–1566.

Bjerknes, J., 1969: Atmospheric teleconnections from the equatorial Pacific. *Mon. Wea. Rev.*, **97**, 163–172.

Cane, M. A., and S. E. Zebiak, 1985: A theory for El Niño and the southern oscillation. *Science*, **228**, 1085–1087, doi: 10.1126/science.228.4703.1085.

Carton, J. A., 1991: Effect of seasonal surface freshwater flux on sea surface temperature in the tropical Atlantic ocean. *J. Geophys. Res.*, **96**, 12 593–12 598, doi: 10.1029/91JC01256.

Deser, C., A. Capotondi, R. Saravanan, and A. S. Phillips, 2006: Tropical Pacific and Atlantic climate variability in CCSM3. *J. Climate*, **19**, 2451–2481, doi: 10.1175/JCLI3759.1.

Gent, P. R., and Coauthors, 2011: The community climate system model version 4. *J. Climate*, **24**, 4973–4991, doi: 10.1175/2011JCLI4083.1.

Gettelman, A., and Coauthors, 2010: Global simulations of ice nucleation and ice supersaturation with an improved cloud scheme in the Community Atmosphere Model. *J. Geophys. Res.*, **115**, D18216, doi: 10.1029/2009JD013797.

Ham, S., and Coauthors, 2012: Effects of freshwater runoff on a tropical Pacific climate in the HadGEM2. *Asia-Pacific Journal of Atmospheric Sciences*, **48**, 457–463.

Huang, B.Y., and V. M. Mehta, 2004: Response of the Indo-Pacific warm pool to interannual variations in net atmospheric freshwater. *J. Geophys. Res.*, **109**, C06022, doi: 10.1029/2003JC002114.

Hunke, E. C., and W. H. Lipscomb, 2008: CICE: The Los Alamos sea ice model user's manual, version 4. Los Alamos National Laboratory Tech. Rep. LA-CC-06-012, 76 pp.

Hurrell, J. W., J. J. Hack, D. Shea, J. M. Caron, and J. Rosinski, 2008: A new sea surface temperature and sea ice boundary dataset for the community atmosphere model. *J. Climate*, **21**, 5145–5153, doi: 10.1175/2008JCLI2292.1.

Kirtman, B. P., Y. Fan, and E. K. Schneider, 2002: The COLA global coupled and anomaly coupled ocean-atmosphere GCM. *J. Climate*, **15**, 2301–2320.

Latif, M., and Coauthors, 1998: A review of the predictability and prediction of ENSO. *J. Geophys. Res.*, **103**, 14 375–14 393, doi: 10.1029/97JC03413.

Mechoso, C. R., and Coauthors, 1995: The seasonal cycle over the tropical Pacific in coupled ocean-atmosphere general circulation models. *Mon. Wea. Rev.*, **123**, 2825–2838.

Neale, R. B., and Coauthors, 2010: Description of the NCAR community atmosphere model (CAM 5.0). NCAR Tech. Note NCAR/TN-486+STR, 274 pp. [Available online at http://www.cesm.ucar.edu/models/cesm1.0/cam/docs/description/cam5_desc.pdf.]

Oleson, K. W., and Coauthors, 2010: Technical description of version 4.0 of the Community Land Model (CLM). NCAR Tech. Note NCAR/TN-478+STR, 257 pp.

Pan, X., B. Huang, and J. Shukla, 2011: Sensitivity of the tropical Pacific seasonal cycle and ENSO to changes in mean state induced by a surface heat flux adjustment in CCSM3. *Climate Dyn.*, **37**, 325–341.

Reason, C. J. C., 1992: On the effect of ENSO precipitation anomalies in a global ocean GCM. *Climate Dyn.*, **8**, 39–47, doi: 10.1007/BF00209342.

Rutt, I. C., M. Hagdorn, N. R. J. Hulton, and A. J. Payne, 2009: The Glimmer community ice sheet model. *J. Geophys. Res.*, **114**, F02004, doi: 10.1029/2008JF001015.

Schlosser, C. A., and P. R. Houser, 2007: Assessing a satellite-era perspective of the global water cycle. *J. Climate*, **20**, 1316–1338.

Smith, R. D., and Coauthors, 2010: The Parallel Ocean Program (POP) reference manual. Los Alamos National Laboratory Tech. Rep. LAUR-10-01853, 140 pp.

Taylor, K. E., R. J. Stouffer, and G. A. Meehl, 2011: An overview of CMIP5 and the experiment design. *Bull. Amer. Meteor. Soc.*, **93**, 485–498, doi: 10.1175/BAMS-D-11-00094.1.

Wu, L., Y. Sun, J. Zhang, L. Zhang, and S. Minobe, 2010: Coupled ocean-atmosphere response to idealized freshwater forcing over the western tropical Pacific. *J. Climate*, **23**, 1945–1954.

Yang, S., K. M. Lau, and P. S. Schopf, 1999: Sensitivity of the tropical Pacific ocean to precipitation-induced freshwater flux. *Climate Dyn.*, **15**, 737–750, doi: 10.1007/s003820050313.

Yu, L., and R. A. Weller, 2007: Objectively analyzed air-sea heat fluxes for the global ice-free oceans (1981–2005). *Bull. Amer. Meteor. Soc.*, **88**, 527–539, doi: 10.1175/BAMS-88-4-527.

Zhang, R.-H., and A. J. Busalacchi, 2008: Rectified effects of tropical instability wave (TIW)-induced atmospheric wind feedback in the tropical Pacific. *Geophys. Res. Lett.*, **35**, L05608,

doi: 10.1029/2007GL033028.

Zhang, R.-H., and A. J. Busalacchi, 2009: Freshwater Flux (FWF)-Induced oceanic feedback in a hybrid coupled model of the tropical Pacific. *J. Climate*, **22**, 853–879, doi: 10.1175/2008JCLI2543.1.

Zhang, R.-H., S. E. Zebiak, R. Kleeman, and N. Keenlyside, 2005: Retrospective El Niño forecasts using an improved intermediate coupled model. *Mon. Wea. Rev.*, **133**, 2777–2802, doi: 10.1175/MWR3000.1.

Zhang, R.-H., A. J. Busalacchi, X. Wang, J. Ballabrera-Poy, R. G. Murtugudde, E. C. Hackert, and D. Chen, 2009: Role of ocean biology-induced climate feedback in the modulation of El Niño-Southern Oscillation. *Geophys. Res. Lett.*, **36**, L03608, doi: 10.1029/2008GL036568.

Zhang, R.-H., G. Wang, D. Chen, A. J. Busalacchi, and E. C. Hackert, 2010: Interannual biases induced by freshwater flux and coupled feedback in the tropical Pacific. *Mon. Wea. Rev.*, **138**, 1715–1737.

Zhang, R.-H., F. Zheng, J. Zhu, Y. Pei, Q. Zheng, and Z. Wang, 2012: Modulation of El Niño-Southern Oscillation by freshwater flux and salinity variability in the Tropical Pacific. *Adv. Atmos. Sci.*, **29**, 647–660, doi: 10.1007/s00376-012-1235-4.

Zhang, R.-H., F. Zheng, J. Zhu, and Z. Wang, 2013: A successful real-time forecast of the 2010–11 La Niña event. *Sci. Rep.*, **3**, 1108, doi: 10.1038/srep01108.

Zheng, F., and R.-H. Zhang, 2012: Effects of interannual salinity variability and freshwater flux forcing on the development of the 2007/08 La Niña event diagnosed from Argo and satellite data. *Dyn. Atmos. Oceans*, **57**, 45–57.

Zheng, F., R.-H. Zhang, and J. Zhu, 2014: Effects of interannual salinity variability on the barrier layer in the western-central equatorial Pacific: A diagnostic analysis from Argo. *Adv. Atmos. Sci.*, **31** (3), 532–542, doi: 10.1007/s00376-013-3061-8.

Zhu, J., B. Huang, M. A. Balmaseda, J. L. Kinter III, P. Peng, Z. -Z. Hu, and L. Marx, 2013: Improved reliability of ENSO hindcasts with multi-ocean analyses ensemble initialization. *Climate Dyn.*, **41**, 2785–2795, doi: 10.1007/s00382-013-1965-8.